

## Weakened Interannual Variability in the Tropical Pacific Ocean since 2000

ZENG-ZHEN HU AND ARUN KUMAR

*NOAA/NWS/NCEP/Climate Prediction Center, College Park, Maryland*

HONG-LI REN

*Department of Meteorology, University of Hawaii at Manoa, Honolulu, Hawaii, and Laboratory for Climate Studies, National Climate Center, China Meteorological Administration, Beijing, China*

HUI WANG

*NOAA/NWS/NCEP/Climate Prediction Center, College Park, Maryland, and WYLE Science, Technology and Engineering Group, McLean, Virginia*

MICHELLE L'HEUREUX

*NOAA/NWS/NCEP/Climate Prediction Center, College Park, Maryland*

FEI-FEI JIN

*Department of Meteorology, University of Hawaii at Manoa, Honolulu, Hawaii*

(Manuscript received 4 May 2012, in final form 4 October 2012)

### ABSTRACT

An interdecadal shift in the variability and mean state of the tropical Pacific Ocean is investigated within the context of changes in El Niño–Southern Oscillation (ENSO). Compared with 1979–99, the interannual variability in the tropical Pacific was significantly weaker in 2000–11, and this shift can be seen by coherent changes in both the tropical atmosphere and ocean. For example, the equatorial thermocline tilt became steeper during 2000–11, which was consistent with positive (negative) sea surface temperature anomalies, increased (decreased) precipitation, and enhanced (suppressed) convection in the western (central and eastern) tropical Pacific, which reflected an intensification of the Walker circulation.

The combination of a steeper thermocline slope with stronger surface trade winds is proposed to have hampered the eastward migration of the warm water along the equatorial Pacific. As a consequence, the variability of the warm water volume was reduced and thus ENSO amplitude also decreased. Sensitivity experiments with the Zebiak–Cane model confirm the link between thermocline slope, wind stress, and the amplitude of ENSO.

### 1. Introduction

Climate across the tropical Pacific Ocean is dominated by interannual variability associated with the El Niño–Southern Oscillation (ENSO). In addition to pronounced interannual variability, there are also significant decadal and interdecadal variations. For example, an ENSO-like change in the global sea surface

temperature (SST) field occurred in the late 1970s, with the evolution marked by an abrupt change toward a warmer tropical eastern Pacific and a colder extratropical central North Pacific (e.g., Nitta and Yamada 1989; Zhang et al. 1997). These low-frequency variations of the tropical Pacific climate may modulate the behavior of ENSO, including its frequency, amplitude, and spatial pattern (Fedorov and Philander 2000; Yeh and Kirtman 2004; Sun and Yu 2009; McPhaden et al. 2011). For example, along with the interdecadal shift in the late 1970s, the ENSO period lengthened from 2–4 yr (high frequency) during 1962–75 to 4–6 yr (low frequency) during 1980–93 (An and Wang 2000). This decadal

---

*Corresponding author address:* Zeng-Zhen Hu, NOAA/NWS/NCEP/Climate Prediction Center, 5830 University Research Court, College Park, MD 20740.  
E-mail: zeng-zhen.hu@noaa.gov

variation has been referred to as an ENSO regime change (Trenberth and Stepaniak 2001; McPhaden and Zhang 2009; Ren and Jin 2011).

Recently, McPhaden (2012) documented another shift around 1999–2000 and reported that while warm water volume (WWV) integrated along the equatorial Pacific led ENSO SST anomalies by two to three seasons during the 1980s and 1990s, WWV variations decreased and lead time was reduced to only one season during the 2000s. Horii et al. (2012) argued that compared with 1981–2000, the interrelationship of the WWV and ENSO became weak after 2000, especially for El Niño–La Niña events during 2005–11. Furthermore, the discharge phases of WWV leading to La Niña events were less frequent beginning in 2001.

Both McPhaden (2012) and Horii et al. (2012) speculated that the breakdown of the relationship between WWV and ENSO may be linked to a shift toward more central Pacific versus eastern Pacific El Niños in the past decade. Based on observations, Xiang et al. (2013) found that since the late 1990s a standing central Pacific warming became the dominant mode in the Pacific and further proposed that it arose from a decadal change characterized by a La Niña-like background pattern. This La Niña-like background pattern was associated with strong divergence in the central Pacific atmospheric boundary layer. They argued that after the late 1990s, the anomalous wind divergence in the central Pacific shifted anomalous convection westward, leading to a westward shift of anomalous westerly response and preventing eastward propagation of the SST anomaly.

In conjunction with these recent studies (e.g., McPhaden 2012; Horii et al. 2012; Xiang et al. 2013), in this work, we further investigate the shift of ENSO variability around 1999–2000 and document the associated coherent changes in the oceanic and atmospheric climate across the tropical Pacific. The data used in the analysis are described in section 2. In section 3, the shift in the variability and mean state of the atmosphere and ocean is investigated, and the connection of the mean-state change with ENSO variability is proposed and tested with a simple model. A summary and implications for ENSO prediction are discussed in section 4.

## 2. Data, model, and sensitivity experiments

### a. Observation-based data

The ocean dataset used in this work is taken from the Global Ocean Data Assimilation System (GODAS; Behringer and Xue 2004). The ocean model in GODAS is based on the Geophysical Fluid Dynamics Laboratory (GFDL) Modular Ocean Model, version 3 (MOM3), in

a quasi-global (75°S–65°N) configuration with specification of climatological sea ice. The spatial resolution is 1° in the zonal direction and 1/3° in the meridional direction between 10°S and 10°N, gradually increasing through the tropics to 1° poleward of 30°S and 30°N. MOM3 has 40 vertical layers with 27 layers in the upper 400 m of the oceans, and it is forced with the atmospheric fluxes from the National Centers for Environmental Prediction (NCEP)/U.S. Department of Energy Global Reanalysis 2 (R2; Kanamitsu et al. 2002). During each assimilation cycle, the model state is corrected by observations within a 4-week window centered on the assimilation time using a three-dimensional variational data assimilation scheme. The observational data assimilated into GODAS include temperature profiles from expendable bathythermographs, Tropical Atmosphere Ocean (TAO), Triangle Trans-Ocean Buoy Network, Pilot Research Moored Array, and Argo profiling floats. Only the temperature data in the top 750 m are assimilated into GODAS.

GODAS monthly mean data are used to analyze ocean temperature and currents along the equator, at the depth of the 20°C isotherm (D20), as well as indices of thermocline slope and WWV. Monthly mean anomalies of the thermocline slope index are computed as the difference in anomalous D20 between the western (160°E–150°W) and eastern (90°–140°W) Pacific. The WWV index is defined as the average of D20 between 5°S–5°N and 120°E–80°W (Meinen and McPhaden 2000).

This analysis is also complemented by the use of ocean temperature profiles of TAO between the ocean surface and 300 m along the equatorial Pacific averaged between 2°S and 2°N. In addition to the comparable mean state and interannual variability of subsurface ocean temperature anomalies (OTAs) between TAO and GODAS (not shown), recently Kumar and Hu (2012a, manuscript submitted to *Climate Dyn.*) showed that the first four leading variability modes of OTA along the equatorial Pacific are almost identical between them. This enhances our confidence in the quality of the reanalyzed GODAS data, which has a longer data record than TAO.

Other observation-based data used in this work include monthly mean SST, precipitation, and outgoing longwave radiation (OLR). The SST data are version 3b of the Extended Reconstructed SST (ERSSTv3b) on a 2° × 2° grid (Smith et al. 2008). ENSO variability is measured using the Niño-3.4 or Niño-3 indices based on ERSSTv3b. The precipitation data are taken from Climate Anomaly Monitoring System and OLR Precipitation Index dataset (CAMS-OPI; Janowiak and Xie 1999) and OLR data are from Liebmann and Smith (1996), both on a 2.5° × 2.5° grid.

Furthermore, we examine the interdecadal shift of the multireanalysis mean of surface wind stress and the Walker circulation from four reanalysis products, including that of the NCEP–National Center for Atmospheric Research (R1; Kalnay et al. 1996), R2 (Kanamitsu et al. 2002), the NCEP Climate Forecast System (CFSR; Saha et al. 2010), and the 25-yr Japan Meteorological Agency (JRA; Onogi et al. 2007) reanalyses. Recent work of Kumar and Hu (2012b) suggested that the multireanalysis mean may be better than any individual reanalysis in describing the air–sea interaction processes associated with ENSO, particularly since quantities like surface heat flux, wind stress, etc., are model-derived variables and are likely model dependent. Therefore, our analysis is based on the multireanalysis mean.

Except for the TAO data from January 1993 to December 2011, and WWV data from January 1980 to December 2011, all the other observation-based analysis or reanalysis data are available for the period from January 1979 to December 2011. All the anomalies are based on the monthly mean climatology of their respective data lengths of each calculation.

### b. Model and sensitivity experiments

To verify the diagnostic results, we design sensitivity experiments using the Zebiak–Cane model (Zebiak and Cane 1987; hereafter referred to as the ZC model), which is a coupled atmosphere–ocean model. The atmospheric component consists of a set of steady-state, linear shallow-water equations on an equatorial beta plane, which is forced by a heating anomaly that depends partially on the SST anomaly and partially on the low-level moisture convergence. The ocean component is a linear reduced-gravity model with a shallow friction layer of constant depth (50 m). Both atmospheric and oceanic components describe perturbations about the observed climatological mean states. See Zebiak and Cane (1987) for details about the model.

For the sensitivity tests, different mean states are generated for model integrations in terms of the perturbed parameter state of the ZC model following the approach of Bejarano and Jin (2008). The perturbed mean states include wind stress and thermocline depth. The basic states are constructed through perturbing the two control parameters,  $\alpha_H$  and  $\alpha_W$ , and altering the referenced upper-layer thickness  $H_0 = \alpha_H H_C$  and the mean wind stress  $(\bar{\tau}^X, \bar{\tau}^Y) = \alpha_W (\bar{\tau}_C^X, \bar{\tau}_C^Y)$ . Here,  $(\bar{\tau}_C^X, \bar{\tau}_C^Y)$  denote the observed climatological mean wind stress, and  $H_C$  is the climatological value for the reference upper-layer thickness. These climatological mean states used here are generated based on observations during 1980–2010. Values of  $\alpha_H$  and  $\alpha_W$  are perturbed so that

$(\bar{\tau}^X, \bar{\tau}^Y)$  varies from 80% to 120% ( $0.8 \leq \alpha_W \leq 1.2$ ) of its observed value with an increment of 1%. Due to the fact that there is no independent parameter in the ZC model to change the thermocline slope directly, instead, we realize this goal of perturbing the thermocline slope indirectly by changing the mean wind stress because they closely correspond to each other. The reason we perturb  $H_0$  is to show the dependence of the ENSO amplitude on thermocline depth, where  $H_0$  alters from 140 to 150 m with an increment of 1 m. For each experiment, the model integrates forward 500 yr, and ENSO standard deviations for the 500 yr are computed as a function of the thermocline slope with parameters varying within a specified range.

## 3. Results

### a. Change in tropical Pacific variability

We first highlight the weaker variability in the Niño-3.4 index and reduced WWV and thermocline slope variability in the tropical Pacific (Fig. 1) since 2000. During January 1980–December 1999, the mean variance was  $0.80$  ( $^{\circ}\text{C}$ )<sup>2</sup> for the Niño-3.4 index,  $706$  m<sup>2</sup> for the thermocline slope index, and  $73.0$  m<sup>2</sup> for the WWV index. During January 2000–December 2011, the corresponding values reduced to  $0.58$  ( $^{\circ}\text{C}$ )<sup>2</sup>,  $412$  m<sup>2</sup>, and  $17.2$  m<sup>2</sup>, respectively (Table 1). Compared with the variance from January 1979 (or from January 1980) to December 1999, the variance in January 2000–December 2011 decreased by 28% for the Niño-3.4 index, by 42% for the thermocline slope index, and by 76% for the WWV index (Table 1). A Monte Carlo test (resampling the data 1000 times with replacement) shows that the chances of randomly achieving larger absolute variance differences between the two periods are 4.4% for the Niño-3.4 index, 0.0% for the thermocline slope index, and 1.6% for the WWV index (Table 1).

Along with the changes in the different aspects that describe ENSO variability, a systematic decrease in the variability for the tropical Pacific climate system was also evident since 2000, including SST, precipitation, and OLR (Figs. 2a–c). The reduction of SST variability is mainly confined to the eastern tropical Pacific (Fig. 2a). A small region of increased SST anomaly variance in the central tropical Pacific (Fig. 2a) is consistent with the findings of Lee and McPhaden (2010) that showed more intense warming events in the central tropical Pacific. The reduction of variability is confined to the central and eastern tropical Pacific for precipitation (Fig. 2b) and OLR (Fig. 2c). We also note a slight enhancement (suppression) of OLR and precipitation variability in the western (northwestern) tropical Pacific

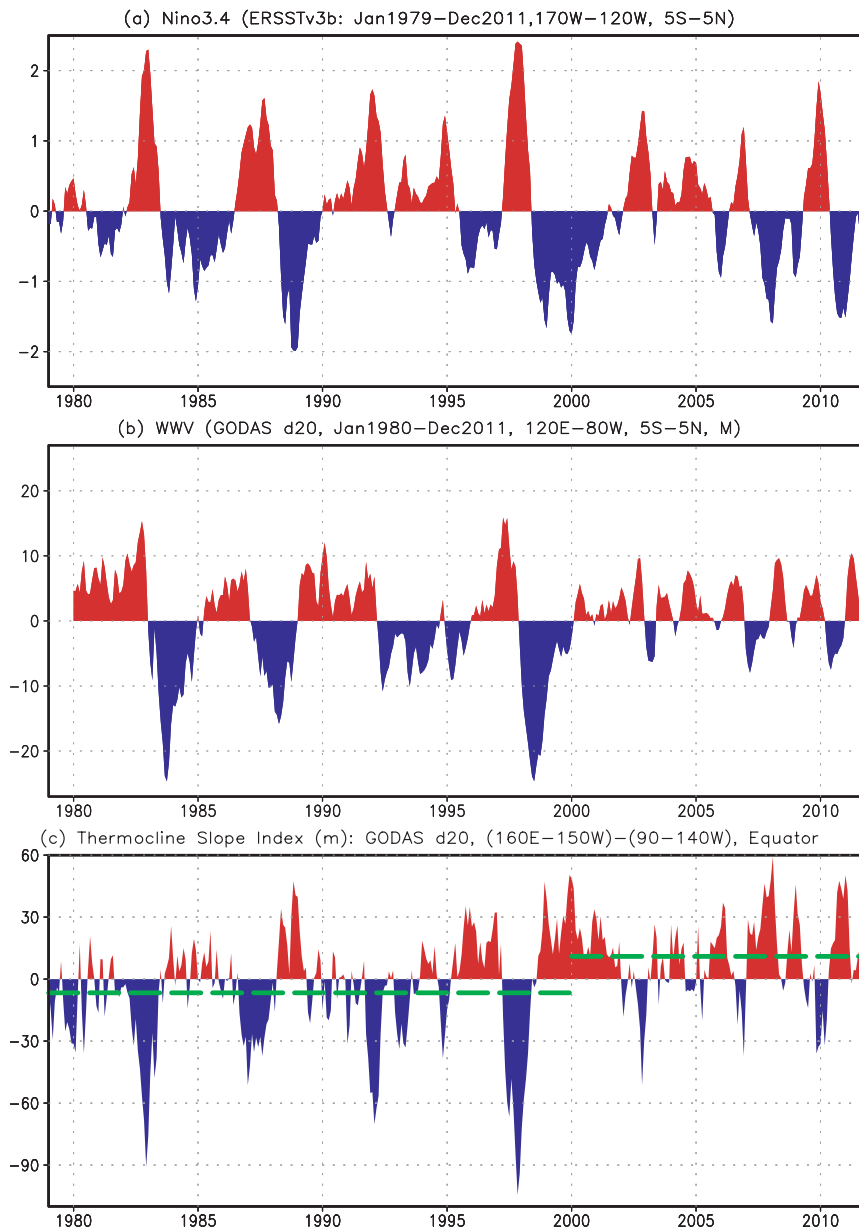


FIG. 1. Monthly mean anomalies of (a) Niño-3.4, (b) WWV, and (c) thermocline slope indices. The mean of the thermocline slope index in Jan 1979–Dec 1999 and Jan 2000–Dec 2011 is shown as dashed lines in (c). The chance of having values larger than or equal to the observed absolute mean differences was found using Monte Carlo testing (through resampling the time series 1000 times) to be 0.0%. The units are degrees Celsius in (a) and meters in (b),(c).

(Figs. 2b,c). The reduction of precipitation and OLR variability in the central basin (Figs. 2b,c) is in line with the reduced SST variability in the eastern tropical Pacific since 2000. On the other hand, the decrease of the D20 variability around 5°S and 5°N in the western Pacific (Fig. 2d) is also consistent with weaker ENSO variability. Recently, Kumar and Hu (2012a, manuscript submitted to *Climate Dyn.*) indicated that the D20 anomalies in these two regions may be linked to ENSO through their connection with the thermocline east–west

The decrease of tropical Pacific climate variability since 2000 is also evident for the thermocline depth along the equatorial Pacific. For instance, we note a decrease in the variability of D20 in the equatorial central

and eastern Pacific (Fig. 2d), suggesting the suppression of thermocline variability along the equatorial Pacific since 2000. On the other hand, the decrease of the D20 variability around 5°S and 5°N in the western Pacific (Fig. 2d) is also consistent with weaker ENSO variability. Recently, Kumar and Hu (2012a, manuscript submitted to *Climate Dyn.*) indicated that the D20 anomalies in these two regions may be linked to ENSO through their connection with the thermocline east–west

TABLE 1. Variances in two periods and the differences, as well as the chance of having values larger than or equal to the absolute values of the observed variance differences using Monte Carlo testing through resampling the respective time series 1000 times.

Index (unit)	1979–99 or 1980–99	2000–11	Differences (relative change to the mean variance in 1979–99 or 1980–99, %)	Chance having larger than or equal to the absolute values of observed variance differences (%)
Niño-3.4 [(°C) <sup>2</sup> ]	0.80	0.58	−0.22 (−28)	4.4
Thermocline slope (m <sup>2</sup> )	706	412	−294 (−42)	0.0
WWV (m <sup>2</sup> )	73.0	17.2	−55.8 (−76)	1.6

oscillation along the equator [the so-called tilt mode; see Figs. 5 and 6 in Kumar and Hu (2012a, manuscript submitted to *Climate Dyn.*)]. In fact, the reduction of OTA variability since 2000 was mainly along the mean thermocline in the central and eastern Pacific (Figs. 3b,d). This is consistent with the variance decrease of the thermocline slope index (Fig. 1c, Table 1) and D20 (Fig. 2d). Due to the fact that the variances in the two periods were computed based on anomalies relative to the means in their respective periods, the impact of mean-state changes on the variance calculation has been eliminated. All these changes document a coherent, weaker variability of the tropical Pacific climate system, including a weakening and a shift in the characteristics of ENSO variability since 2000.

#### b. Change in the mean state

In concert with the reduced variability of the ocean–atmosphere system in the tropical Pacific, the mean state also experienced a marked shift around 1999–2000. The difference of OTA between post- and pre-2000 consists of mainly positive changes above the thermocline in the western Pacific, and primarily negative anomalies below the thermocline in the eastern Pacific (Figs. 3a,c). These changes result in a sharpening tendency of the vertical gradient of the ocean temperature along the thermocline. Moreover, the OTA differences (Figs. 3a,c) indicate a tendency toward a steeper thermocline tilt during 2000–11. The steepening tendency of the thermocline tilt since 2000 is largely due to deepening of the thermocline in the equatorial western Pacific, whereas the shoaling of the thermocline in the equatorial eastern Pacific is relatively small. The steeper thermocline tilt is also seen in the thermocline slope index shown in Fig. 1c: the mean state shifts from below normal to above normal around 1998–2000 (Fig. 1c). Furthermore, the thermocline tilt shift is also observed when the thermocline tilt index is defined as the east–west difference of thermocline depth with maximum vertical temperature gradient (not shown). That provides an additional piece of evidence for the thermocline slope shift.

In addition to changes in the equatorial Pacific thermocline (Figs. 3a,c) since 2000, there were warmer (colder)

SSTs (Fig. 4a), increased (decreased) precipitation (Fig. 4b), and enhanced (suppressed) convection (Fig. 4c) in the western (central and eastern) tropical Pacific, as well as intensified equatorial trade winds (Fig. 4d). As a result, this change leads to an enhanced zonal SST gradient (Fig. 4a). Also, compared to the climatology of OLR and precipitation (contours in Figs. 4b,c), both the OLR and precipitation differences (shadings in Figs. 4b,c) suggest a slight northward shift of the intertropical convergence zone (ITCZ) in the central and eastern tropical Pacific and a strengthening and northwestward shift over the northwestern Pacific. This is collocated with change in the surface divergence (shading in Fig. 4d) implied by the change in the surface wind stress.

Therefore, the reduction of the variability is in conjunction with the overall changes of the mean state, including a stronger Walker circulation (Fig. 5). All four reanalyses show the same overall Walker circulation tendency, with anomalous ascending motion over the western equatorial Pacific and anomalous descending motion in the eastern Pacific, although there are differences in the details among the reanalyses (Fig. 5). For instance, CFSR lacks a significant region of subsidence east of the International Date Line, but still reflects increased ascending motion over Indonesia and the western Pacific. The overall consistent pattern among the four reanalyses enhances the credibility that the Walker circulation is strengthening in this period, which is distinctive from the longer-term weakening of the Walker circulation indicated in Vecchi et al. (2006). In fact, changes in the Walker circulation depend on the time scales examined and, sometime, on the data sources as well (Vecchi et al. 2006; Meng et al. 2012).

The coherent mean-state changes of the atmospheric and oceanic components may suggest a role for coupling and feedback processes. For example, since 2000, warming SSTs in the west and cooling temperatures in the east, as well as an increase in the zonal SST gradient, lead to an increase (decrease) in precipitation and enhanced (suppressed) convection (OLR) in the western (eastern) equatorial Pacific. Such changes enhance the surface winds and strengthen the Walker circulation, which, in turn, can increase the thermocline slope. Given

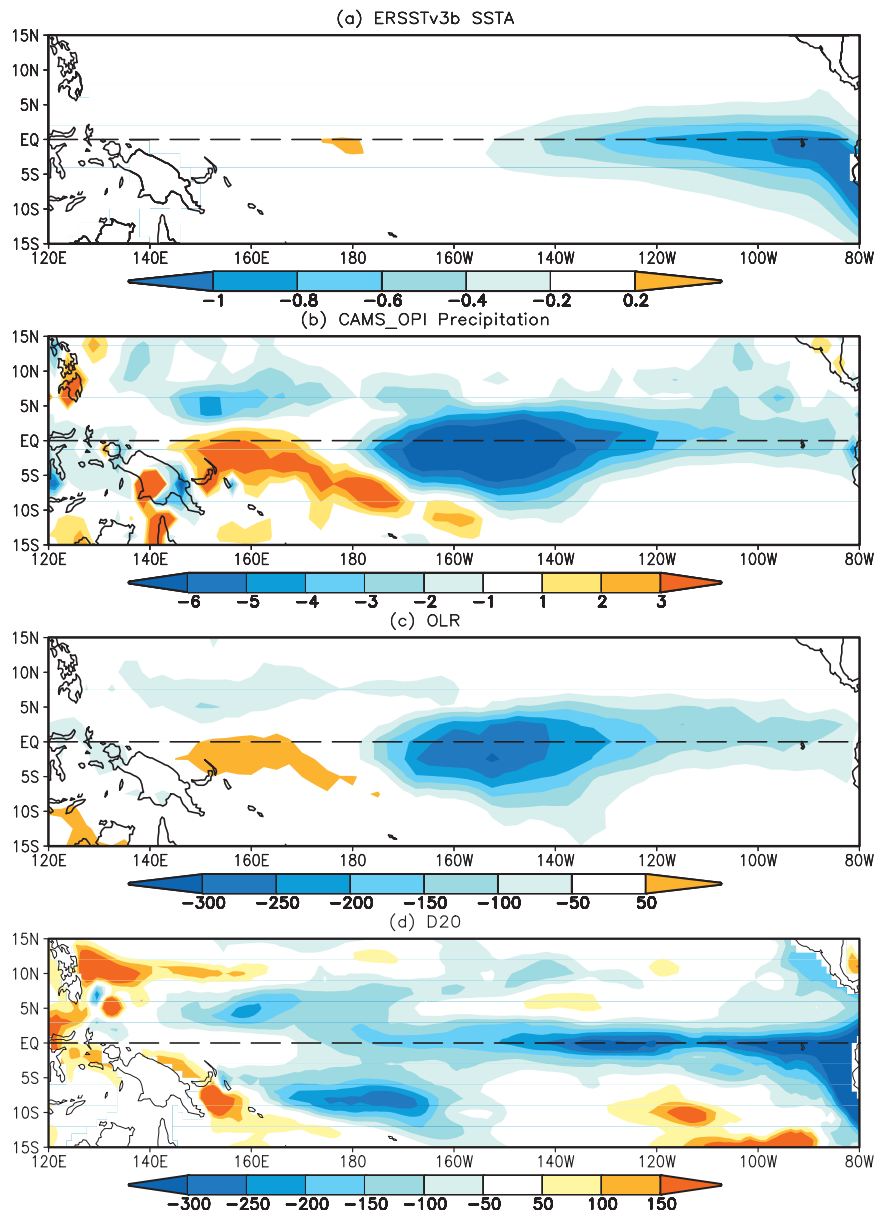


FIG. 2. Variance differences of (a) ERSSTv3b SSTA, (b) CAMS-OPI precipitation, (c) OLR, and (d) D20 between the means in Jan 2000–Dec 2011 and in Jan 1979–Dec 1999. The units are degrees Celsius squared in (a), millimeters per day squared in (b), watts per square meter squared in (c), and square meters in (d).

the changes in the mean state of the tropical Pacific, a natural question is whether such changes in the mean state may be responsible for variability changes of the tropical Pacific climate, including ENSO.

### c. Verification using the ZC model

It has been documented that ENSO behavior varies with regimes of the tropical atmosphere–ocean coupled system (Jin and Neelin 1993; Neelin and Jin 1993) and are sensitive to the mean state of the coupled system.

Fedorov and Philander (2000, 2001) suggested that mean wind and thermocline depth changes are associated with SST variability changes along the equator. Bejarano and Jin (2008) further documented the dependence of ENSO modes on the equatorial Pacific mean-state changes using a linearized ZC model. Choi et al. (2009) indicated that decadal-varying tropical Pacific SST and thermocline depth anomalies are significantly correlated with decadal variations of the ENSO amplitudes in a coupled general circulation model.

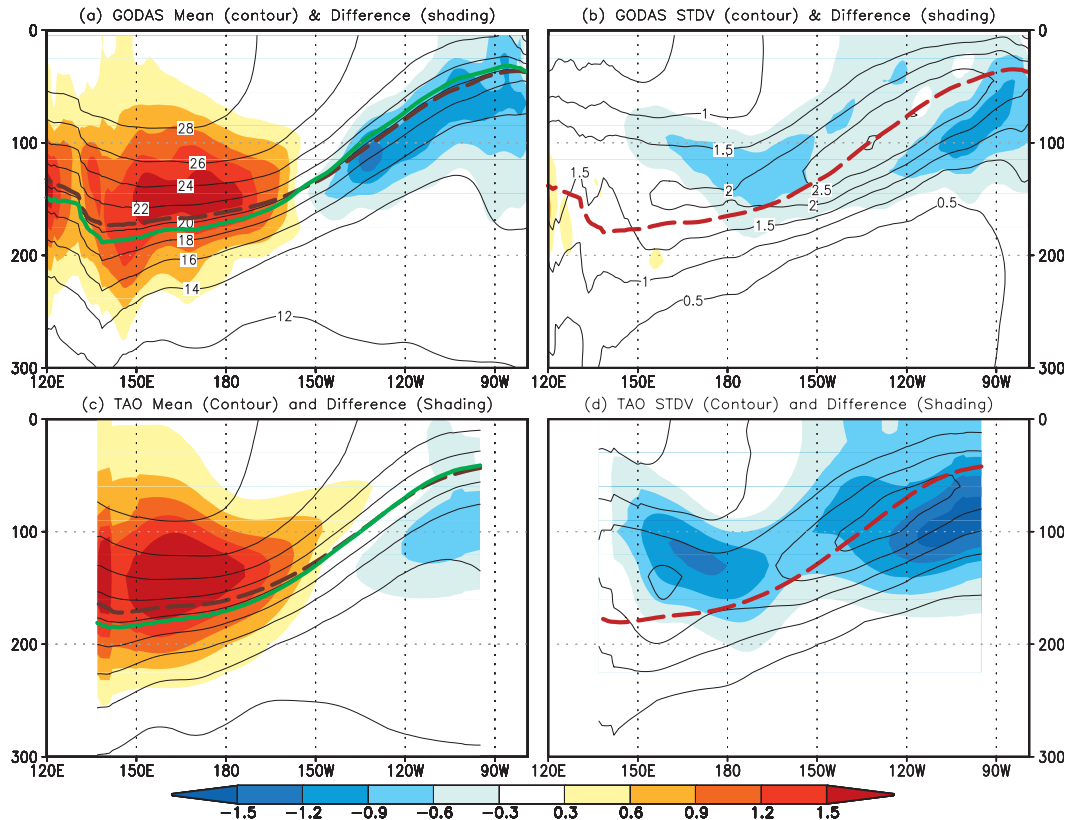


FIG. 3. (a) Mean (contours) and its difference (shading) and (b) std dev (contours) and its difference (shading) of GODAS ocean temperature along the equatorial Pacific averaged between  $2^{\circ}\text{S}$  and  $2^{\circ}\text{N}$  varied with ocean depth and longitude. (c),(d) As in (a),(b), respectively, but for TAO data. The mean is the average in Jan 1979–Dec 2011 for GODAS data, and in Jan 1993–Dec 2011 for TAO data. The difference is between Jan 2000–Dec 2011 and Jan 1979–Dec 1999 for GODAS data, and between Jan 2000–Dec 2011 and Jan 1993–Dec 1999 for TAO data. The thick dashed (solid) line is the mean D20 in Jan 1979–Dec 1999 (Jan 2000–Dec 2011) for GODAS in (a), in Jan 1993–Dec 1999 (Jan 2000–Dec 2011) for TAO in (c), in Jan 1979–Dec 2011 for GODAS in (b), and in Jan 1993–Dec 2011 for TAO in (d). Contour intervals are  $2^{\circ}\text{C}$  in (a),(c) and  $0.5^{\circ}\text{C}$  in (b),(d).

Here, we hypothesize that the combination of the enhanced trade wind and thermocline slope may restrict the eastward extension of the warm pool beyond the central equatorial Pacific to the eastern equatorial Pacific. As a consequence, ENSO variability decreases. This hypothesis is tested by 451 sensitivity experiments with different thermocline depth and wind stress intensity parameters using the ZC model (Zebiak and Cane 1987). Figure 6 shows the dependence of the Niño-3 index standard deviation on the slope of equatorial thermocline over  $125^{\circ}\text{E}$ – $85^{\circ}\text{W}$  in the ZC model and in the observations. To compare the model results with observations, we display the relative thermocline slope ( $y$  axis) and Niño-3 index standard deviation ( $x$  axis). For the model simulations, the relative thermocline slope is defined as the result of the mean thermocline slope in each experiment divided by the average slope in all experiments. This is similar to the Niño-3 index standard deviation. In the observations, the relative thermocline

slope (Niño-3 index standard deviation) is the result of the mean thermocline slope (Niño-3 index standard deviation) in either 1979–99 or 2000–11 divided by the mean in 1979–2011. Each dot in Fig. 6 represents a 500-yr average for one experiment. The plus sign (relative Niño-3 index standard deviation = 1.08, relative thermocline slope = 0.94) corresponds to the observed values in 1979–99, and the triangle (relative Niño-3 index standard deviation = 0.84, relative thermocline slope = 1.12) to the observed values in 2000–11.

The spread of dots in Fig. 6 is due to the variations by perturbing the thermocline depth and surface wind stress parameters. There is a relatively flat top near the maxima with a broad range straddling the relative thermocline slope of 1. It is unclear why the maximum ENSO amplitude tends to occur at the mean thermocline slope of the model. Nevertheless, the overall distribution pattern shown in Fig. 6 suggests that as the thermocline slope increases, ENSO variability grows

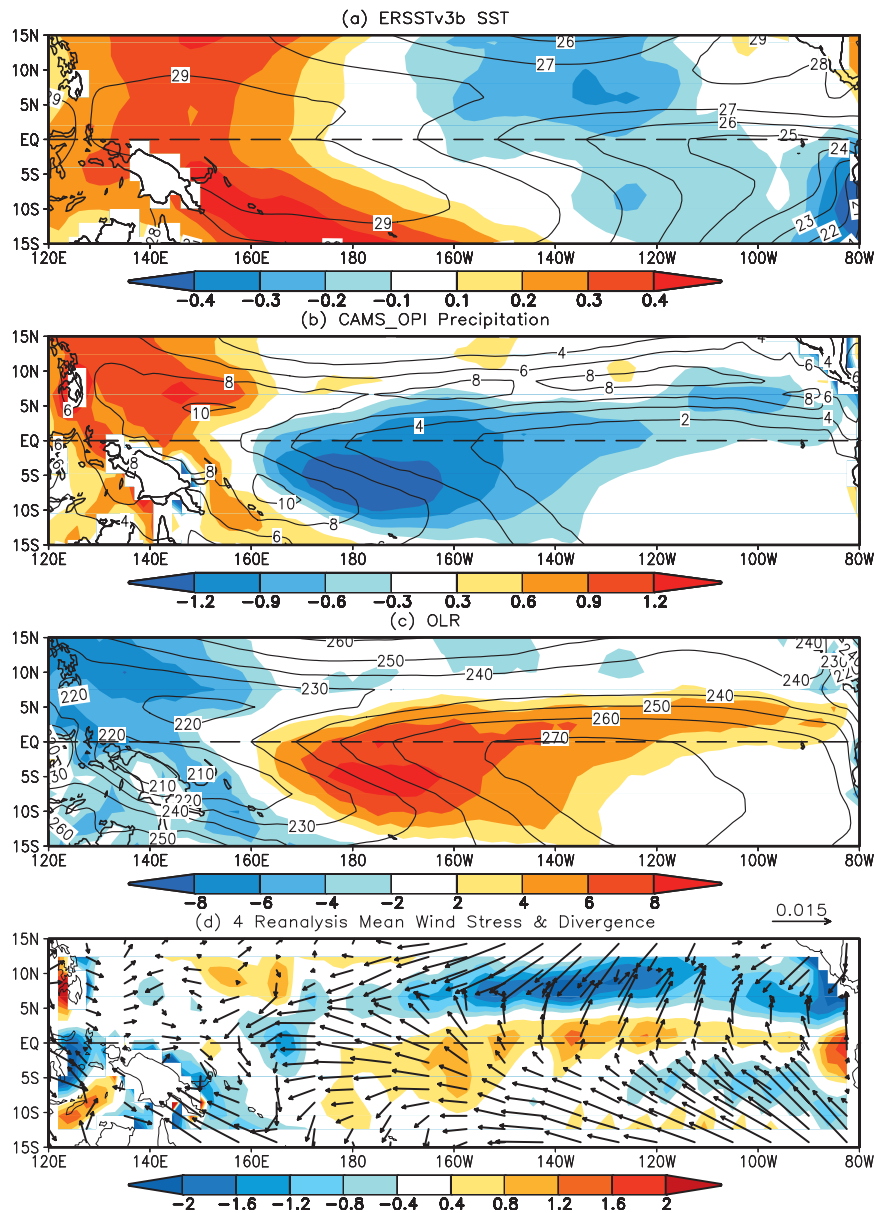


FIG. 4. Differences (shading) and mean (contours) of (a) ERSSTv3b SST, (b) CAMS-OPI precipitation, and (c) OLR, and differences of (d) surface wind stress (vectors) and its divergence (shading). The differences are between the averages in Jan 2000–Dec 2011 and Jan 1979–Dec 1999, and the means are for Jan 1979–Dec 2011. The surface wind stress is the two-period difference averaged for the four reanalyses: R1, R2, CFSR, and JRA. The units are degrees Celsius in (a), millimeters per day in (b), watts per square meter in (c), and newtons per square meter for the surface wind stress (and  $10^{-8} \text{ N m}^{-3}$ ) for the divergence in (d).

and then weakens after the peak (Fig. 6). This confirms the hypothesis that either too strong or too weak thermocline slope (trade winds) results in small ENSO variability. This result is also consistent with previous work. For example, Fedorov and Philander (2000) pointed out that either too strong or too weak mean wind (either too large or too small thermocline slope)

may generate a smaller growth rate and thus weaker ENSO. They argued that the presence of the delayed oscillation mode (having a period of several years) requires zonal wind of a certain intensity and a thermocline in the eastern Pacific that is neither too shallow nor too deep. Because the deeper the thermocline, the smaller the direct influence of the wind on SST variations. In



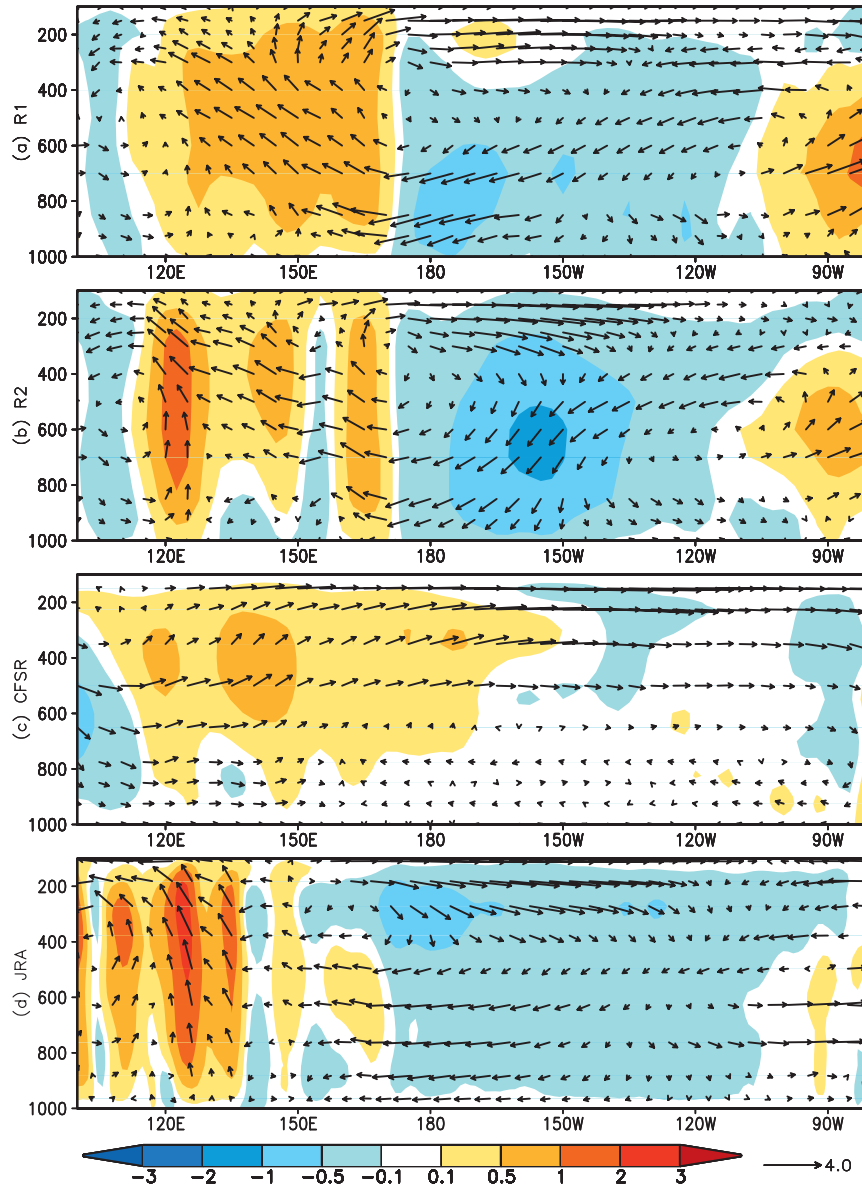


FIG. 5. Differences of the Walker circulation (vectors) and atmospheric vertical velocity (shading) averaged over  $5^{\circ}\text{S}$ – $5^{\circ}\text{N}$  between the means in Jan 2000–Dec 2011 and Jan 1979–Dec 1999 for (a) R1, (b) R2, (c) CFSR, and (d) JRA. The units are meters per second for the zonal component and pascals per second for the vertical velocity. In the plots, we enlarge the vertical velocity values by 50 times and also reverse the sign.

addition, when the thermocline is too deep (trade winds are too weak), its vertical movements have little impact on SST so that ocean–atmosphere interactions are precluded. On the other hand, when the thermocline is too shallow (trade winds are too strong), the mean surface temperature in the eastern Pacific drops thus reducing the vertical temperature gradients and weakening the ENSO variability.

The observations during 1979–99 were in a regime with a relatively small-to-medium thermocline slope and wind stress, and large ENSO variability (Fig. 6). In

contrast, since 2000, the observations have moved into a regime with a larger thermocline slope and wind stress and, therefore, smaller ENSO variability. The results based on the ZC model experiments show the significant standard deviation difference between the two periods. Thus, the model results support our hypothesis: a thermocline slope that is either too large or too small (with too strong or too weak wind stress) along the equator could suppress ENSO variability. Nevertheless, the large spread in the Niño-3 variance for a relative thermocline

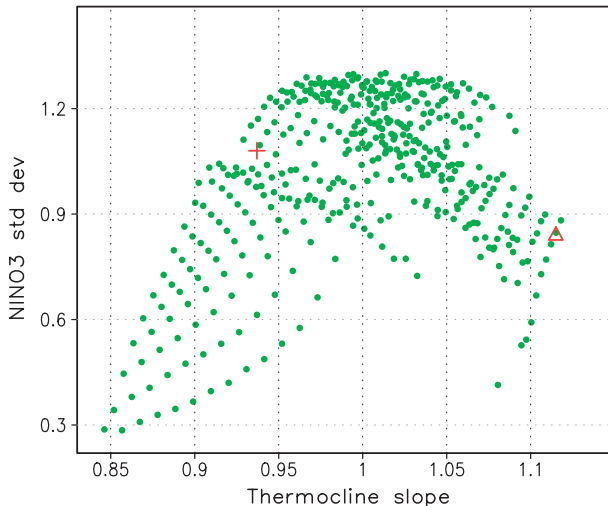


FIG. 6. Dependence of 500-yr-averaged relative Niño-3 index std dev (y axis) on the relative thermocline slope (x axis) between 125°E and 85°W along the equator in the ZC model. The thermocline slope here reflects the combined influence of changes in wind stress and thermocline depth along the equatorial Pacific Ocean. The red plus sign (at 1.08, 0.94) denotes the corresponding values for the observed mean relative Niño-3 index std dev and the relative thermocline slope in 1979–99, and the red triangle (at 0.84, 1.12) shows the observed mean in 2000–11.

slope around one in Fig. 6 may imply that in addition to the thermocline slope, other factors such as the vertical temperature gradient and mean thermocline depth may also play a role in ENSO variability change.

We also note that after 2000 the ENSO frequency became relatively higher, in conjunction with the mean-state shift to a shallow thermocline in the eastern tropical Pacific and stronger trade winds. This observed evidence is consistent with the simple model results of Fedorov and Philander (2001). They argued that the ENSO period increased from approximately 3 to 5 yr from the 1960s to the 1990s because of the decadal fluctuation of mean states with a deeper thermocline in the eastern tropical Pacific and weaker trade winds. However, we did not find a clear conclusion about the impacts of mean-state change on the ENSO period in the model sensitivity experiments, which may be due to the multiplicity of ENSO behaviors with mean-state change (e.g., Bejarano and Jin 2008), as well as the simplicity of the model compared to the real climate system. The relationship between mean state and ENSO period is an interesting but a complicated topic, which merits further study.

#### 4. Summary and discussion

In this work, we investigated the interdecadal change in the variability and mean state in the tropical Pacific

within the context of ENSO. Compared with 1979–99, the interannual variability in the tropical Pacific was significantly weaker during 2000–11. There was a change toward a steeper thermocline tilt during 1979–2011, which was consistent with the positive (negative) SST anomaly, above (below) normal precipitation, and enhanced (suppressed) convection in the western (central and eastern) tropical Pacific, as well as a change toward intensified trade winds and a more energetic Walker circulation. These mean-state changes suggest a slightly northward shift of the ITCZ in the central and eastern tropical Pacific and a stronger tendency and northwestward shift of the ITCZ over the northwestern Pacific.

According to Meinen and McPhaden (2000) and Jin (1997a,b), the cyclic nature of ENSO is caused by a disequilibrium between zonal winds and zonal mean thermocline depth. We speculate that the combination of enhanced trade winds and a steeper thermocline slope since 2000 may make the eastward extension of the warm pool along the equatorial Pacific more difficult. As a consequence, the canonical El Niño cannot fully develop in the eastern Pacific and ENSO-related tropical Pacific variability decreased. This hypothesized link between the trade winds and the thermocline with ENSO amplitude is verified by sensitivity experiments of long-term integration of the Zebiak and Cane model. It is shown that either too large or too small of a thermocline slope (and too strong or too weak a wind stress) along the equator can lead to a reduction in ENSO amplitude, and may provide an explanation for consistent changes between the mean state and ENSO. There is no doubt that the results might be dependent on the model. On the other hand, the observation-based dataset may still not be long enough to provide robust statistics. For example, Stevenson et al. (2010) argued that measuring ENSO variability with 90% confidence requires approximately 240 yr of observations. Therefore, it is necessary to examine this hypothesis using different models with varying complexity and longer data records.

This hypothesis is supported by an oceanic circulation change along the equator. Compared with the mean in January 1979–December 1999, anomalous upward motion is seen in the central and western Pacific, and anomalous downward motion in the central and eastern Pacific during January 2000–December 2011 (not shown). Nevertheless, it is unclear how the ocean circulation change is connected with the Walker circulation change. The ocean circulation change may reduce the thermocline feedback in the eastern Pacific due to the anomalous downward motion, and also prevent the subsurface warm water residing in the western Pacific from propagating into the eastern Pacific. That is consistent with the evidence of a more frequent occurrence of a central Pacific

El Niño in the recent decades, which is also in line with recent work of Xiang et al. (2013). They argued that strong divergence in the central Pacific atmospheric boundary layer after the late 1990s prevented the eastward propagation of SST anomalies.

The relationship between ENSO amplitude and the mean state, however, is still an open question (Meehl et al. 2001; Fedorov and Philander 2001; Wang and An 2002; Hu et al. 2004), requiring further theoretical and modeling analysis. For example, from this work, we note that the vertical temperature gradient in the thermocline region became sharper since 2000, in conjunction with a decrease in ENSO amplitude. However, Collins (2000) suggested that the increase in the vertical temperature gradient, associated with a model's response to increased greenhouse gases, is responsible for an increase in the amplitude of ENSO. In addition to the impact of the mean state, the sensitivity of the atmosphere to the ocean also affects the ENSO amplitude. Vecchi and Wittenberg (2010) argued that if winds respond strongly to SST, ENSO tends to be more active, whereas if clouds over the eastern equatorial Pacific respond strongly to SST, ENSO tends to be less active.

Moreover, the causes of changes in the mean state and ENSO amplitude are still controversial. Were these changes just a manifestation of the natural variability in the climate system, or can they be linked to external causes? Wittenberg (2009) noted strong interdecadal and intercentennial modulation of ENSO, which can change the ENSO variance upward of 100% in a 2000-yr GFDL coupled-model free run where atmospheric composition, solar irradiance, and land cover were held fixed at 1860 values. That suggests that variations internal to the ocean-atmosphere system can produce changes in the mean state and ENSO amplitude. However, besides the natural variations, the increase in the greenhouse gas (GHG) concentrations is also a potential contributor to the changes in the mean state and characteristics of ENSO variability (Collins et al. 2010; Latif and Keenlyside 2008; Meehl et al. 2006; Jin et al. 2001). For instance, under the influence of increasing GHG concentrations, it was argued that the tropical easterly trade winds will weaken, the equatorial thermocline will shoal, and the temperature gradients across the thermocline will become larger (Collins et al. 2010). Hu et al. (2012) showed a weakening of the variability associated with ENSO in a coupled model simulation under the global warming scenario. Meehl et al. (2006) argued that the observed phenomenon of more frequent and stronger El Niño events occurs only in the initial phase of global warming, and after the lower layers of the ocean get warmer as well, El Niño variability becomes smaller than it once was. This is consistent with

the findings of Hu et al. (2000), who showed a variance increase in Niño-3 SST during an earlier period of a global warming scenario simulation and a decrease in the later period (see Fig. 2d in Hu et al. 2000). These studies may imply that the ocean stratification or vertical temperature gradient across the thermocline is important for the frequency and intensity of ENSO (Collins 2000; Thual et al. 2011). Overall, it seems that both the natural and GHG-forced mean-state changes can modify ENSO features, and natural variability, at times, can override the signal associated with the external forcing.

It has been suggested that decadal-interdecadal variations in the tropical Pacific mean state can modulate ENSO behavior and affect the prediction skills of ENSO. For example, in a simple coupled model, Kirtman and Schopf (1998) showed that during decades with large (small) amplitude of the interannual variability, the forecast skill of ENSO is relatively high (low) and the limit of predictability is relatively long (short). Wang et al. (2010) argued that the SST forecast skill in the eastern and central tropical Pacific is a function of the amplitude of the interannual variability of the tropical Pacific SST: larger (smaller) variability of the SST anomaly corresponding to higher (lower) skill levels of the SST anomaly in the Niño-3.4 region (see Fig. 5 in Wang et al. 2010). The change in the characteristics of ENSO variability since 2000 has also been reflected in the prediction skill of ENSO in various seasonal prediction systems (Wang et al. 2010; Barnston et al. 2012). The skill change is associated with the reduced predictability of low-amplitude and higher-frequency events, reflecting a smaller signal-to-noise ratio that may lead to less predictability. This decadal change in forecast skill is likely associated with the variation of ENSO amplitude discussed in this work.

*Acknowledgments.* We appreciate the comments and suggestions from the reviewers, as well as Soon-II An, Rong-Hua Zhang, Wanqiu Wang, Peitao Peng, Caihong Wen, and Jian Li. Ren and Jin are supported by DOE Grant DE-SC0005110, the 973 Program of China (2010CB950404), NOAA Grant NA10OAR4310200, and National Science Foundation Grant ATM 1034798.

## REFERENCES

- An, S.-I., and B. Wang, 2000: Interdecadal change of the structure of the ENSO mode and its impact on the ENSO frequency. *J. Climate*, **13**, 2044–2055.
- Barnston, A. G., M. K. Tippett, M. L. L'Heureux, S. Li, and D. G. DeWitt, 2012: Skill of real-time seasonal ENSO model predictions during 2002–11: Is our capability increasing? *Bull. Amer. Meteor. Soc.*, **93**, 631–651.
- Behringer, D. W., and Y. Xue, 2004: Evaluation of the Global Ocean Data Assimilation System at NCEP: The Pacific Ocean. Preprints, *Eighth Symp. on Integrated Observing and*

- Assimilation Systems for Atmosphere, Oceans, and Land Surface*, Seattle, WA, Amer. Meteor. Soc., 2.3. [Available online at <http://ams.confex.com/ams/pdfpapers/70720.pdf>.]
- Bejarano, L., and F.-F. Jin, 2008: Coexistence of equatorial coupled modes of ENSO. *J. Climate*, **21**, 3051–3067.
- Choi, J., S.-I. An, B. Dewitte, and W.-W. Hsieh, 2009: Interactive feedback between the tropical Pacific decadal oscillation and ENSO in a coupled general circulation model. *J. Climate*, **22**, 6597–6611.
- Collins, M., 2000: The El Niño–Southern Oscillation in the second Hadley Centre coupled model and its response to greenhouse warming. *J. Climate*, **13**, 1299–1312.
- , and Coauthors, 2010: The impact of global warming on the tropical Pacific Ocean and El Niño. *Nat. Geosci.*, **3**, 391–397, doi:10.1038/ngeo868.
- Fedorov, A. V., and S. G. Philander, 2000: Is El Niño changing? *Science*, **288**, 1997–2002.
- , and —, 2001: A stability analysis of tropical ocean–atmosphere interactions: Bridging measurements and theory for El Niño. *J. Climate*, **14**, 3086–3101.
- Horii, T., I. Ueki, and K. Hanawa, 2012: Breakdown of ENSO predictors in the 2000s: Decadal changes of recharge/discharge–SST phase relation and atmospheric intraseasonal forcing. *Geophys. Res. Lett.*, **39**, L10707, doi:10.1029/2012GL051740.
- Hu, Z.-Z., M. Latif, E. Roeckner, and L. Bengtsson, 2000: Intensified Asian summer monsoon and its variability in a coupled model forced by increasing greenhouse gas concentrations. *Geophys. Res. Lett.*, **27**, 2681–2684.
- , E. K. Schneider, U. S. Bhatt, and B. P. Kirtman, 2004: Potential mechanism for response of El Niño–Southern Oscillation variability to change in land surface energy budget. *J. Geophys. Res.*, **109**, D21113, doi:10.1029/2004JD004771.
- , A. Kumar, B. Jha, and B. Huang, 2012: An analysis of forced and internal variability in a warmer climate in CCSM3. *J. Climate*, **25**, 2356–2373.
- Janowiak, J. E., and P. Xie, 1999: CAMS–OPI: A global satellite–rain gauge merged product for real-time precipitation monitoring applications. *J. Climate*, **12**, 3335–3342.
- Jin, F.-F., 1997a: An equatorial ocean recharge paradigm for ENSO. Part I: Conceptual model. *J. Atmos. Sci.*, **54**, 811–829.
- , 1997b: An equatorial ocean recharge paradigm for ENSO. Part II: A stripped-down coupled model. *J. Atmos. Sci.*, **54**, 830–847.
- , and J.-D. Neelin, 1993: Modes of interannual tropical ocean–atmosphere interaction—A unified view. Part I: Numerical results. *J. Atmos. Sci.*, **50**, 3477–3503.
- , Z.-Z. Hu, M. Latif, L. Bengtsson, and E. Roeckner, 2001: Dynamics and cloud–radiation feedbacks in El Niño and greenhouse warming. *Geophys. Res. Lett.*, **28**, 1539–1542.
- Kalnay, E., and Coauthors, 1996: The NCEP/NCAR 40-Year Reanalysis Project. *Bull. Amer. Meteor. Soc.*, **77**, 437–471.
- Kanamitsu, M., and Coauthors, 2002: NCEP–DOE AMIP-II Reanalysis (R-2). *Bull. Amer. Meteor.*, **83**, 1631–1643.
- Kirtman, B. P., and P. S. Schopf, 1998: Decadal variability in ENSO predictability and prediction. *J. Climate*, **11**, 2804–2822.
- Kumar, A., and Z.-Z. Hu, 2012b: Uncertainty in the ocean–atmosphere feedbacks associated with ENSO in the reanalysis products. *Climate Dyn.*, **39**, 575–588, doi:10.1007/s00382-011-1104-3.
- Latif, M., and N. Keenlyside, 2008: El Niño/Southern Oscillation response to global warming. *Proc. Natl. Acad. Sci. USA*, **106**, 20 578–20 583, doi:10.1073/pnas.0710860105.
- Lee, T., and M. J. McPhaden, 2010: Increasing intensity of El Niño in the central equatorial Pacific. *Geophys. Res. Lett.*, **37**, L14603, doi:10.1029/2010GL044007.
- Liebmann, B., and C. A. Smith, 1996: Description of a complete (interpolated) outgoing long wave radiation dataset. *Bull. Amer. Meteor. Soc.*, **77**, 1275–1277.
- McPhaden, M. J., 2012: A 21st century shift in the relationship between ENSO SST and warm water volume anomalies. *Geophys. Res. Lett.*, **39**, L09706, doi:10.1029/2012GL051826.
- , and X. Zhang, 2009: Asymmetry in zonal phase propagation of ENSO sea surface temperature anomalies. *Geophys. Res. Lett.*, **36**, L13703, doi:10.1029/2009GL038774.
- , T. Lee, and D. McClurg, 2011: El Niño and its relationship to changing background conditions in the tropical Pacific Ocean. *Geophys. Res. Lett.*, **38**, L15709, doi:10.1029/2011GL048275.
- Meehl, G. A., P. R. Gent, J. M. Arblaster, B. L. Otto-Bliesner, E. C. Brady, and A. Craig, 2001: Factors that affect amplitude of El Niño in global coupled climate models. *Climate Dyn.*, **17**, 515–526.
- , H. Teng, and G. Branstator, 2006: Future changes of El Niño in two global coupled climate models. *Climate Dyn.*, **26**, 549–566, doi:10.1007/s00382-005-0098-0.
- Meinen, C. S., and M. J. McPhaden, 2000: Observations of warm water volume changes in the equatorial Pacific and their relationship to El Niño and La Niña. *J. Climate*, **13**, 3551–3559.
- Meng, Q., M. Latif, W. Park, N. S. Keenlyside, V. A. Semenov, and T. Martin, 2012: Twentieth-century Walker circulation change: Data analysis and model experiments. *Climate Dyn.*, **38**, 1757–1773, doi:10.1007/s00382-011-1047-8.
- Neelin, J. D., and F.-F. Jin, 1993: Modes of interannual tropical ocean–atmosphere interaction—A unified view. Part II: Analytical results in the weak coupling limit. *J. Atmos. Sci.*, **50**, 3504–3522.
- Nitta, T., and S. Yamada, 1989: Recent warming of tropical sea surface temperature and its relationship to the Northern Hemisphere circulation. *J. Meteor. Soc. Japan*, **67**, 375–383.
- Onogi, K., and Coauthors, 2007: The JRA-25 Reanalysis. *J. Meteor. Soc. Japan*, **85**, 369–432.
- Ren, H.-L., and F.-F. Jin, 2011: Niño indices for two types of ENSO. *Geophys. Res. Lett.*, **38**, L04704, doi:10.1029/2010GL046031.
- Saha, S., and Coauthors, 2010: The NCEP Climate Forecast System Reanalysis. *Bull. Amer. Meteor. Soc.*, **91**, 1015–1057.
- Smith, T. M., R. W. Reynolds, T. C. Peterson, and J. Lawrimore, 2008: Improvements to NOAA’s historical merged land–ocean surface temperature analysis (1880–2006). *J. Climate*, **21**, 2283–2296.
- Stevenson, S., B. Fox-Kemper, M. Jochum, B. Rajagopalan, and S. G. Yeager, 2010: ENSO model validation using wavelet probability analysis. *J. Climate*, **23**, 5540–5547.
- Sun, F., and J.-Y. Yu, 2009: A 10–15-yr modulation cycle of ENSO intensity. *J. Climate*, **22**, 1718–1735.
- Thual, S., B. Dewitte, S.-I. An, and N. Ayoub, 2011: Sensitivity of ENSO to stratification in a recharge–discharge conceptual model. *J. Climate*, **24**, 4332–4349.
- Trenberth, K. E., and D. P. Stepaniak, 2001: Indices of El Niño evolution. *J. Climate*, **14**, 1697–1701.
- Vecchi, G. A., and A. T. Wittenberg, 2010: El Niño and our future climate: Where do we stand? *Wiley Interdiscip. Rev.: Climate Change*, **1**, 260–270, doi:10.1002/wcc.33.
- , B. J. Soden, A. T. Wittenberg, I. M. Held, A. Leetmaa, and M. J. Harrison, 2006: Weakening of tropical Pacific atmospheric circulation due to anthropogenic forcing. *Nature*, **441**, 73–76.

- Wang, B., and S.-I. An, 2002: A mechanism for decadal changes of ENSO behavior: Roles of background wind changes. *Climate Dyn.*, **18**, 475–486.
- Wang, W., M. Chen, and A. Kumar, 2010: An assessment of the CFS real-time seasonal forecasts. *Wea. Forecasting*, **25**, 950–969.
- Wittenberg, A. T., 2009: Are historical records sufficient to constrain ENSO simulations? *Geophys. Res. Lett.*, **36**, L12702, doi:10.1029/2009GL038710.
- Xiang, B., B. Wang, and T. Li, 2013: A new paradigm for the predominance of standing central Pacific warming after the late 1990s. *Climate Dyn.*, doi:10.1007/s00382-012-1427-8, in press.
- Yeh, S. W., and B. P. Kirtman, 2004: Tropical Pacific decadal variability and ENSO amplitude modulation in a CGCM. *J. Geophys. Res.*, **109**, C11009, doi:10.1029/2004JC002442.
- Zebiak, S. E., and M. A. Cane, 1987: A model El Niño/Southern Oscillation. *Mon. Wea. Rev.*, **115**, 2262–2278.
- Zhang, Y., J. M. Wallace, and D. S. Battisti, 1997: ENSO-like interdecadal variability: 1900–93. *J. Climate*, **10**, 1004–1020.